

# RSC Advances



This is an *Accepted Manuscript*, which has been through the Royal Society of Chemistry peer review process and has been accepted for publication.

*Accepted Manuscripts* are published online shortly after acceptance, before technical editing, formatting and proof reading. Using this free service, authors can make their results available to the community, in citable form, before we publish the edited article. This *Accepted Manuscript* will be replaced by the edited, formatted and paginated article as soon as this is available.

You can find more information about *Accepted Manuscripts* in the [Information for Authors](#).

Please note that technical editing may introduce minor changes to the text and/or graphics, which may alter content. The journal's standard [Terms & Conditions](#) and the [Ethical guidelines](#) still apply. In no event shall the Royal Society of Chemistry be held responsible for any errors or omissions in this *Accepted Manuscript* or any consequences arising from the use of any information it contains.

**Synthesis, characterization and photocatalytic activity of magnetically separable  $\gamma$ -Fe<sub>2</sub>O<sub>3</sub>/N,Fe codoped TiO<sub>2</sub> heterojunction for degradation of Reactive Blue 4 dye**

**Navneet Kaur<sup>a</sup>, Satwant Kaur<sup>a,b</sup>, Vasundhara Singh<sup>a</sup>**

<sup>a</sup>Department of Applied Sciences (Chemistry), PEC University of Technology, Chandigarh 160012, INDIA

email: navneetpuchem88@gmail.com; Tel.No.-91-9646765448, vasun7@yahoo.co.in, Tel. No.-91-172-2733263

<sup>b</sup>Department of Chemistry, ASBASJSM College, Bela, Ropar 140001, INDIA

email: shahi.satwant@yahoo.com; Tel. No.-91-9815620645



**Synthesis, characterization and photocatalytic activity of magnetically separable  $\gamma$ -Fe<sub>2</sub>O<sub>3</sub>/N,Fe codoped TiO<sub>2</sub> heterojunction for degradation of Reactive Blue 4 dye**

**Navneet Kaur<sup>a</sup>, Satwant Kaur<sup>a,b</sup>, Vasundhara Singh<sup>a</sup>**

*<sup>a</sup>Department of Applied Sciences (Chemistry), PEC University of Technology, Chandigarh 160012, INDIA*

*email: navneetpuchem88@gmail.com; Tel.No.-91-9646765448, vasun7@yahoo.co.in, Tel. No.-91-172-2733263*

*<sup>b</sup>Department of Chemistry, ASBASJSM College, Bela, Ropar 140001, INDIA*

*email: shahi.satwant@yahoo.com; Tel. No.-91-9815620645*

### **Abstract**

In the present work, nanocrystalline undoped, N-doped and N,Fe codoped TiO<sub>2</sub> have been synthesized by sol-gel method for the photocatalytic degradation of Reactive Blue 4 dye under visible light, with N,Fe codoped TiO<sub>2</sub> exhibiting the best activity. Further, to encounter the problem of separation of N,Fe codoped TiO<sub>2</sub> photocatalyst, magnetically separable  $\gamma$ -Fe<sub>2</sub>O<sub>3</sub>/N,Fe codoped TiO<sub>2</sub> heterojunction was fabricated and found to exhibit enhanced photoactivity with 100% dye degradation as compared to 85% with N,Fe codoped TiO<sub>2</sub>. This behavior has been attributed to the facilitated electron-hole transfer in  $\gamma$ -Fe<sub>2</sub>O<sub>3</sub>/N,Fe codoped TiO<sub>2</sub> heterojunction, low electron-hole recombination rate, existence of pure anatase phase and a narrow band gap of 1.5eV. The recycled  $\gamma$ -Fe<sub>2</sub>O<sub>3</sub>/N,Fe codoped TiO<sub>2</sub> also demonstrated good repeatability of photoactivity. The mechanism involved for degradation of dye by  $\gamma$ -Fe<sub>2</sub>O<sub>3</sub>/N,Fe codoped TiO<sub>2</sub> has also been discussed. In conclusion, the synthesis of magnetically separable and visible light active titania by coupling of  $\gamma$ -Fe<sub>2</sub>O<sub>3</sub> and N,Fe codoped TiO<sub>2</sub> to overcome its limitations of narrow band gap and non-recyclability with additional advantage of enhanced photocatalytic activity for degradation of Reactive Blue 4 dye has been achieved.

**Keywords:** heterojunction, magnetically separable photocatalyst, N,Fe codoped TiO<sub>2</sub>, photocatalytic activity, visible light

## 1. Introduction

Semiconductor photocatalysts, mainly TiO<sub>2</sub>, has attracted much attention in the last decade for the removal of organic and inorganic pollutants<sup>1-4</sup> because of its high activity, chemical stability, commercial availability and non-toxicity. However, TiO<sub>2</sub> inevitably encounter two obstacles when applied in practice which are, narrow light response and difficulty in separation.<sup>5</sup> Therefore, the development of a visible light active (VLA) and magnetically separable photocatalyst has become an important topic of research in this field.

The doping of non-metals or metals in TiO<sub>2</sub><sup>6-11</sup> resulted in efficient photoactivity in the visible region. Recently, codoped TiO<sub>2</sub> with non-metals and metals has been investigated, which are found to be even more promising to make TiO<sub>2</sub> visible light responsive.<sup>12,13</sup> Among the various combinations of non-metal and metal codoping, nitrogen and iron codoping has received considerable attention because of their interesting synergistic effect in depressing the electron-hole recombination rate.<sup>14,15</sup>

An approach to overcome the separation problem is by the synthesis of a photocatalyst via incorporating magnetic nanoparticles due to the ease of their removal by the application of an external magnetic field.<sup>16</sup> Unfortunately, sometimes photo-dissolution of catalyst may occur, leading to the separation of TiO<sub>2</sub> from the magnetic iron oxide core, which not only changes the properties of the magnetic iron oxides but also decreases the photocatalytic activity.<sup>17,18</sup> Several papers have been reported in literature on the synthesis of TiO<sub>2</sub>-based magnetic photocatalysts<sup>19,20</sup> but research in the synthesis of magnetically separable VLA titania is still in its infancy and very few papers with magnetically separable non-metal or metal doped TiO<sub>2</sub> have

been reported.<sup>21-23</sup> Yu et al recently reported magnetically separable N,La codoped TiO<sub>2</sub> as the first report of the synthesis with non-metal and metal codoped TiO<sub>2</sub>.<sup>24</sup>

In this paper, the visible light induced photodegradation study has been carried out for Reactive Blue 4 dye (RB 4) with undoped, N-doped and N,Fe codoped TiO<sub>2</sub>. The best activity was found with N,Fe codoped TiO<sub>2</sub> which was further modified for the improvement in the separation process of the photocatalyst as magnetically separable  $\gamma$ -Fe<sub>2</sub>O<sub>3</sub>/N,Fe codoped TiO<sub>2</sub>.<sup>25,26</sup> The enhanced photoactivity of  $\gamma$ -Fe<sub>2</sub>O<sub>3</sub>/N,Fe codoped TiO<sub>2</sub> has been accounted for based on the suggested mechanism and its physico-chemical properties.

## 2. Experimental

### 2.1. Reagents and Chemicals

Tetrabutyl titanate (TBT), Fe(NO<sub>3</sub>)<sub>3</sub>.9H<sub>2</sub>O, FeSO<sub>4</sub>, urea and RB 4 dye (M.W. = 637.43 gmol<sup>-1</sup>, C.I. 61205) were purchased from Sigma-Aldrich, USA. All other chemicals, ammonium hydroxide (NH<sub>3</sub>.H<sub>2</sub>O, 25-28%), acetic acid, absolute ethanol were of analytical grade and used as received without any further purification. Double distilled water (DDW) was used throughout the study.

### 2.2. Preparation of modified photocatalysts

#### 2.2.1. Synthesis of $\gamma$ -Fe<sub>2</sub>O<sub>3</sub>

A mixture of 0.18M of Fe(NO<sub>3</sub>)<sub>3</sub>.9H<sub>2</sub>O (50ml) and 0.12M of FeSO<sub>4</sub> (50ml) solution were mechanically stirred at 40°C and followed by the addition of NH<sub>3</sub>.H<sub>2</sub>O (5ml). The mixture was stirred for 15 min and heated at 60°C for 10 min. The black precipitates formed were separated with a magnet and washed with double distilled water (4x20ml). The as-obtained precipitates of iron oxide were finally heated at 100°C to form stable  $\gamma$ -Fe<sub>2</sub>O<sub>3</sub> as a dry powder.

### 2.2.2. Preparation of undoped, N-doped and N,Fe codoped TiO<sub>2</sub>

Firstly, TBT (5 ml) and acetic acid (5 ml) were added in 25 ml of absolute ethanol (solution A). Secondly, acetic acid (2.5 ml) and distilled water (3 ml) were added in 12.5 ml of absolute ethanol (solution B). Solution B was added drop-wise into the solution A with vigorous magnetic agitation. The obtained mixture was stirred for 3 h, followed by drying at 100°C in the oven, porphyzied into a powder and then annealed at 500°C at a rate of 3°C per minute in a programmable furnace for 3 h. The final powder obtained was undoped TiO<sub>2</sub>. The N-doped and N,Fe codoped TiO<sub>2</sub> were prepared with the same procedure by using dopant sources, urea (1.8 g, 30 mmol) and ferric nitrate (0.17 g, 0.43 mmol) for nitrogen and iron respectively, added in solution B.

### 2.2.3. Preparation of $\gamma$ -Fe<sub>2</sub>O<sub>3</sub>/N,Fe codoped TiO<sub>2</sub>

$\gamma$ -Fe<sub>2</sub>O<sub>3</sub> (0.77 g, 4.82 mmol) was added in solution A in the above procedure to obtain  $\gamma$ -Fe<sub>2</sub>O<sub>3</sub>/N,Fe codoped TiO<sub>2</sub> catalyst. The schematic process for synthesis of modified TiO<sub>2</sub> has been shown in **Fig. 1**.

The as-synthesized materials were characterized by X-ray diffraction (XRD), Transmission Electron Microscope (TEM), Brunauer Emmett Teller (BET), Fourier Transform Infra-red spectra (FTIR), UV-vis diffuse reflectance spectra (UV-vis DRS), X-ray photoelectron spectroscopy (XPS) and Energy dispersive X-ray spectra (EDS) techniques.

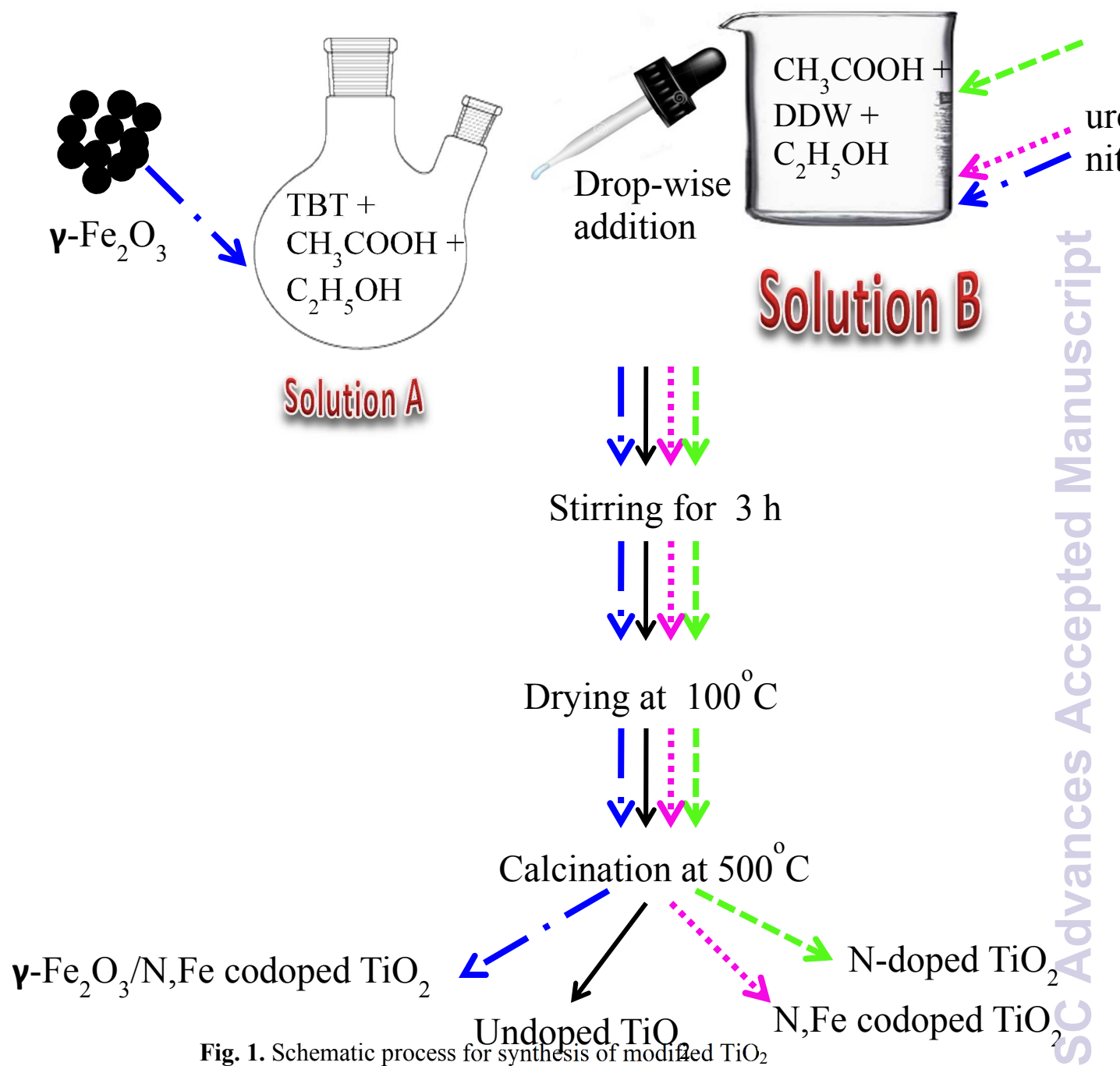


**Fig. 1.** Schematic process for synthesis of modified  $\text{TiO}_2$

### 2.3. Characterization of nanocrystalline $\text{TiO}_2$

XRD measurements were performed using an X-ray powder diffractometer (XPRT-PRO) operated at 45 kV and 40 mA with Cu-K $\alpha$  radiation ( $\lambda=0.15406$  nm) at a scan angle ( $2\theta$ ) of 20-100°. TEM images of samples were studied using transmission electron microscope of Hitachi

(H- 7500) with an accelerating voltage of 120 kV. EDS was performed with EDX-INCAx-act, Oxford instrument, attached with TEM. The hydrodynamic particle sizes were determined from Malvern Zetasizer ZS90. BET surface area measurements were performed using Quantachrome Nova Win version 10.01 and the samples were previously outgassed at 180<sup>0</sup>C for 2 h. FTIR in the range 4000-400 cm<sup>-1</sup> were taken from Perkin Elmer - Spectrum RX-I. UV-vis DRS of samples were performed on a Perkin Elmer-Lambda 35 UV-vis spectrophotometer, with a double-beam optical arrangement, equipped with an integrating sphere attachment. The BaSO<sub>4</sub> was used as a reference.<sup>27</sup> XPS was recorded with a Shimadzu ESCA-3200 spectrometer. The shift of binding energy due to relative surface charging was corrected using the C1s level at 284.6 eV as an internal standard.

#### 2.4. Photocatalytic experiments

The photocatalytic experiments were performed with 200 ml of dye solution in an immersion well type reactor. The experiments were conducted using a 100W halogen lamp with the circulation of 2 M NaNO<sub>2</sub> solution for absorption of any irradiation below 400 nm with vigorous bubbling of oxygen into the solution to increase the dissolved oxygen concentration. An aliquot of 5 ml was taken from the reactor at regular intervals of time with a syringe. The suspension was centrifuged for 5 min at 4000 rpm and subsequently filtered through a Millipore filter (pore size 0.45µm) to remove the catalyst and the filtrate was analyzed by UV-vis spectrophotometer.

### 3. Characterization

**Fig. 2** shows the XRD pattern of all the synthesized photocatalysts. The XRD patterns shown in **Fig. 2a**, **2b** and **2c**, corresponds to undoped, N-doped TiO<sub>2</sub> and N,Fe codoped TiO<sub>2</sub> respectively, indicating the presence of anatase phase (JCPDS No. of pure anatase- 01-071-1167) only in undoped and N-doped TiO<sub>2</sub> while in case of N,Fe codoped TiO<sub>2</sub>, it has anatase phase

with trace amount of rutile phase (JCPDS No. of pure rutile- 01-078-1510) i.e. 95.55% anatase and 4.45% rutile phase<sup>28</sup> as calculated by the following equation -

$$F_A = 100 - \frac{1}{1 + \frac{0.81 I_A}{I_R}} 100$$

where  $I_A$  is the intensity of the 101 peak of anatase and  $I_R$  is the intensity of the 110 peak of rutile.

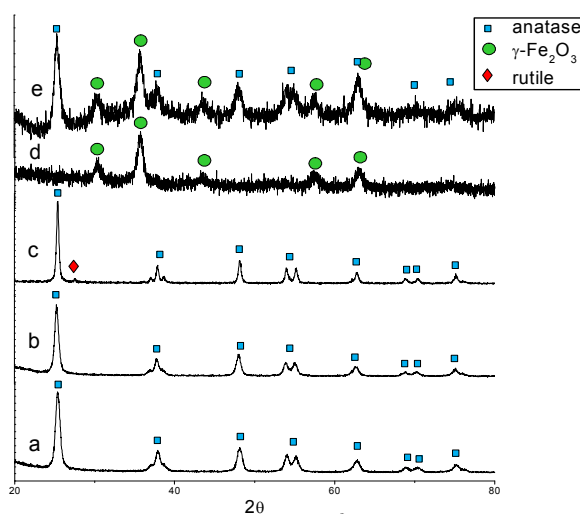


**Fig. 2.** XRD patterns of the synthesized photocatalysts calcined at 500°C (a) undoped TiO<sub>2</sub>, (b) N-doped TiO<sub>2</sub>, (c) N,Fe codoped TiO<sub>2</sub>, (d)  $\gamma$ -Fe<sub>2</sub>O<sub>3</sub> and (e)  $\gamma$ -Fe<sub>2</sub>O<sub>3</sub>/N,Fe codoped TiO<sub>2</sub>.

The XRD diffraction peaks  $\gamma$ -Fe<sub>2</sub>O<sub>3</sub> in **Fig. 2d** at  $2\theta = 30.29^\circ, 35.72^\circ, 43.40^\circ, 57.45^\circ, 63.07^\circ$  and  $74.6^\circ$  confirms its crystal lattice structure.<sup>21</sup> The diffraction peaks in **Fig. 2e** of  $\gamma$ -Fe<sub>2</sub>O<sub>3</sub>/N,Fe codoped TiO<sub>2</sub>, showed the anatase peaks of TiO<sub>2</sub> and the peaks of  $\gamma$ -Fe<sub>2</sub>O<sub>3</sub> which remains unchanged, and reveals that the magnetic properties are not lost after high temperature treatment. The absence of rutile phase in **Fig. 2e** as compared to **Fig. 2c** suggests that there is some interaction between  $\gamma$ -Fe<sub>2</sub>O<sub>3</sub> and N,Fe codoped TiO<sub>2</sub>.

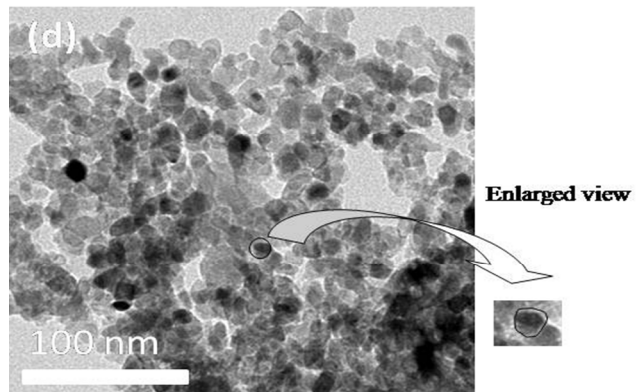
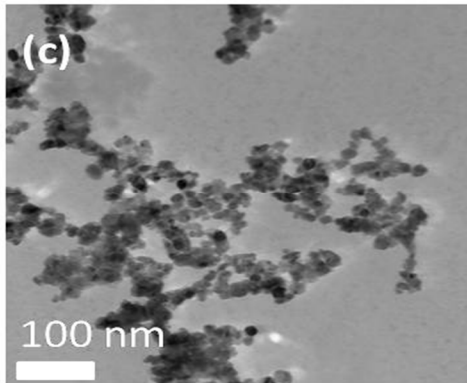
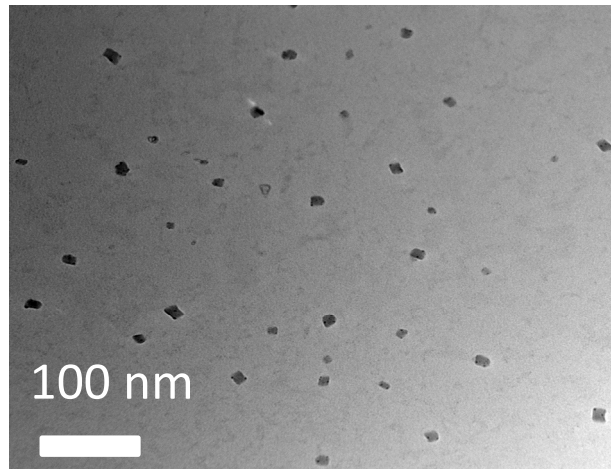
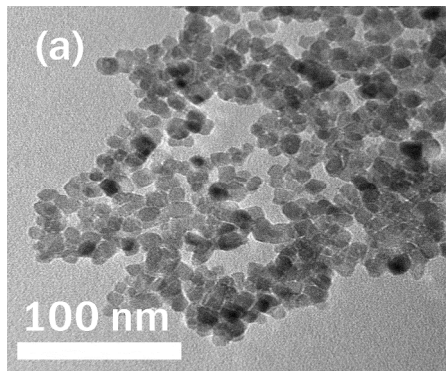
The crystallite sizes of all photocatalysts were calculated by Debye-Scherrer equation as shown in **Table 1**.

**Table 1.** Physico-chemical properties of synthesized photocatalysts.

	Undoped TiO <sub>2</sub>	N-doped TiO <sub>2</sub>	N,Fe codoped TiO <sub>2</sub>	$\gamma$ -Fe <sub>2</sub> O <sub>3</sub> /N,Fe codoped TiO <sub>2</sub>
Crystallite size(nm) from XRD	14.2	13.6	21.3	12.0
Range of particle size(nm) from TEM	8-15	12-18	9-12	7-14
Hydrodynamic size (Å)	238.8	132.8	25.2	42.0
Band gap (eV)	3.0	2.6	2.4	1.5
BET surface area (m <sup>2</sup> g <sup>-1</sup> )	103.8	83.4	98.0	131.5

**Fig. 3.** illustrates the TEM images of all synthesized samples. The particle size from TEM was found to be in agreement with the crystallite size calculated from XRD analysis. The undoped and N,Fe codoped TiO<sub>2</sub> (**Fig. 3a and 3c**) have a cubic shape while N-doped TiO<sub>2</sub> (**Fig. 3b**) showed rectangular shape with low aggregation of particles. **Fig. 3d** of  $\gamma$ -Fe<sub>2</sub>O<sub>3</sub>/N,Fe codoped TiO<sub>2</sub> showed heterogeneous dispersion of ultrafine  $\gamma$ -Fe<sub>2</sub>O<sub>3</sub> magnetic nanoparticles in

the N,Fe codoped TiO<sub>2</sub> matrix.<sup>29</sup> The heterojunction formed between  $\gamma$ -Fe<sub>2</sub>O<sub>3</sub> and N,Fe codoped TiO<sub>2</sub> has been shown in the enlarged view of **Fig. 3d**. The dark region corresponds to  $\gamma$ -Fe<sub>2</sub>O<sub>3</sub> and the light region corresponds to N,Fe codoped TiO<sub>2</sub>. The presence of well defined SAED ring pattern in HRTEM of  $\gamma$ -Fe<sub>2</sub>O<sub>3</sub>/N,Fe codoped TiO<sub>2</sub> confirmed the crystallinity of titania. Further, the calculated d-spacing of 0.35 nm and 0.25 nm corresponding to the (101) plane of anatase of TiO<sub>2</sub> and (110) plane of Fe<sub>2</sub>O<sub>3</sub> respectively confirmed the presence of heterojunction as shown in **Fig. 3e**.



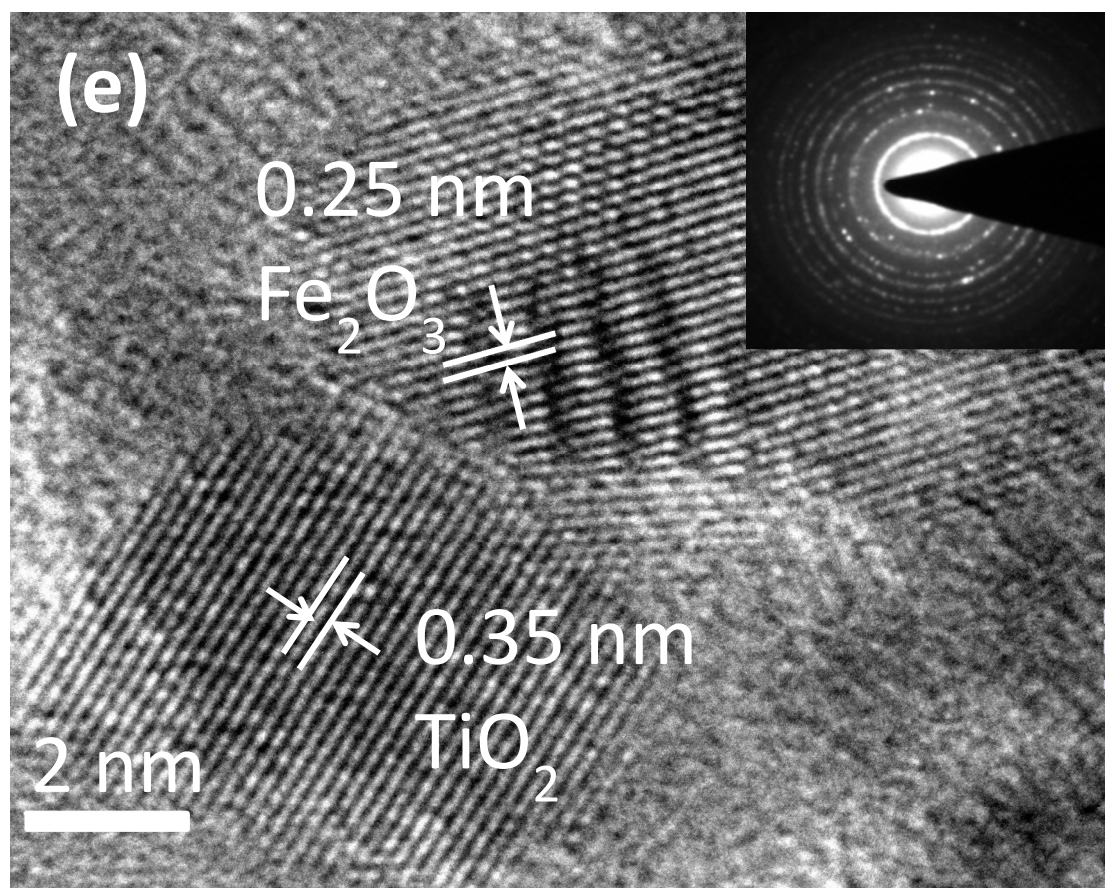


**Fig.3.** TEM images of (a) undoped  $\text{TiO}_2$ , (b) N-doped  $\text{TiO}_2$ , (c) N,Fe codoped  $\text{TiO}_2$ , (d)  $\gamma\text{-Fe}_2\text{O}_3/\text{N,Fe}$  codoped  $\text{TiO}_2$  and (e) HRTEM of  $\gamma\text{-Fe}_2\text{O}_3/\text{N,Fe}$  codoped  $\text{TiO}_2$

The hydrodynamic particle size of all the synthesized  $\text{TiO}_2$  samples has also been determined as given in **Table 1**. The hydrodynamic sizes of the photocatalysts were found to be larger than the crystallite size, calculated by Debye-Scherrer equation, due to the aggregation of the powders in an aqueous media.

The BET surface area of the synthesized samples are shown in **Table 1**. Among all the samples,  $\gamma\text{-Fe}_2\text{O}_3/\text{N,Fe}$  codoped  $\text{TiO}_2$  has higher surface area which can be accounted for based on the different nucleation and growth of nanocrystallites resulting in the formation of particles of small size and correspondingly having larger surface area.<sup>30</sup>

The FTIR spectra has been analyzed of all samples to confirm the composition and structure of nanocomposites (**Fig. 4**). In all the spectra, the peaks at 1620 and 3400  $\text{cm}^{-1}$  are attributed to absorption by water and hydroxyl groups<sup>31</sup> and peaks at 500-900  $\text{cm}^{-1}$  originates from Ti-O-Ti bond.<sup>32</sup> The small peaks at around 1450, 1230 and 1090  $\text{cm}^{-1}$  can be assigned to the nitrogen atoms embedded in the  $\text{TiO}_2$  network in doped  $\text{TiO}_2$  samples. In the spectra of  $\gamma\text{-Fe}_2\text{O}_3/\text{N,Fe}$  codoped  $\text{TiO}_2$ , the peak around 570  $\text{cm}^{-1}$  was observed which is due to the vibration of Fe-O bond.

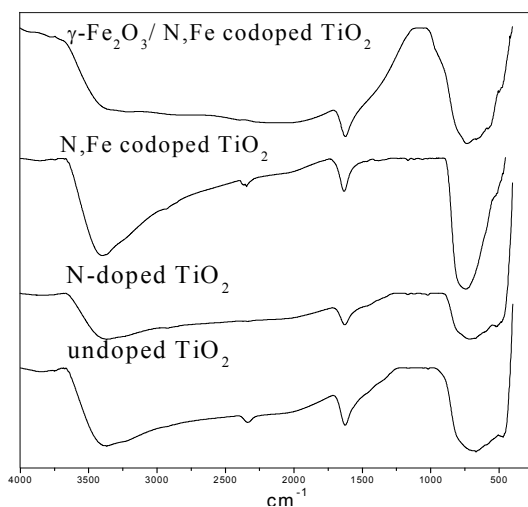


**Fig. 4.** FTIR spectra of the synthesized photocatalysts

**Fig. 5** showed the UV-vis DRS spectra of all synthesized catalysts and their band gap was calculated by Tauc plot.<sup>33</sup> The undoped  $\text{TiO}_2$  has a band gap of 3.0 eV indicating that it can absorb only UV light. In N-doped  $\text{TiO}_2$ , the band gap shifts from 3.0 eV to 2.6 eV because of hybridization of N 2p with O 2p orbitals. In N,Fe codoped  $\text{TiO}_2$ , the incorporation of iron further decreases the band gap to 2.4 eV.<sup>34</sup> The doping of nitrogen and iron in  $\text{TiO}_2$  forms the impurity band just above the valence band (VB) and below the conduction band (CB) respectively in  $\text{TiO}_2$ .<sup>35</sup> The reduction in band gap confirms that both nitrogen and iron weave efficiently into the

crystal lattice structure. In  $\gamma$ -Fe<sub>2</sub>O<sub>3</sub>/N,Fe codoped TiO<sub>2</sub>, the band gap further lowers to 1.5 eV which justifies their increased absorption in the visible region.<sup>36</sup> The shift in band gap might be due to the formation of a heterojunction between  $\gamma$ -Fe<sub>2</sub>O<sub>3</sub> and N,Fe codoped TiO<sub>2</sub> which was further confirmed from HRTEM analysis. This is further supported by literature reports where heterojunction formation leads to reduction in band gap.<sup>37-39</sup>

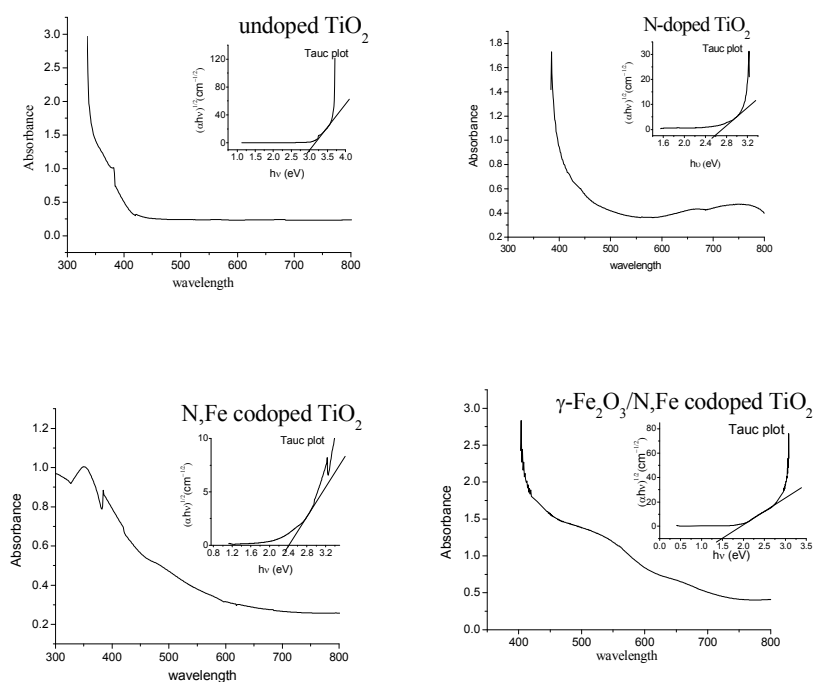


**Fig. 5.** UV-vis DRS analysis of the synthesized photocatalysts.

The XPS spectra of doped samples as represented in **Fig. 6**, showed a clear N 1s binding energy around 400 eV which has been assigned to interstitial nitrogen and residual non-influent N species at the surface.<sup>40-42</sup> The N,Fe codoped TiO<sub>2</sub> sample showed peaks for the binding energies of Fe 2p located at 722.6 and 709.7 eV indicating the existence of Fe-O bond on the surface of the sample.

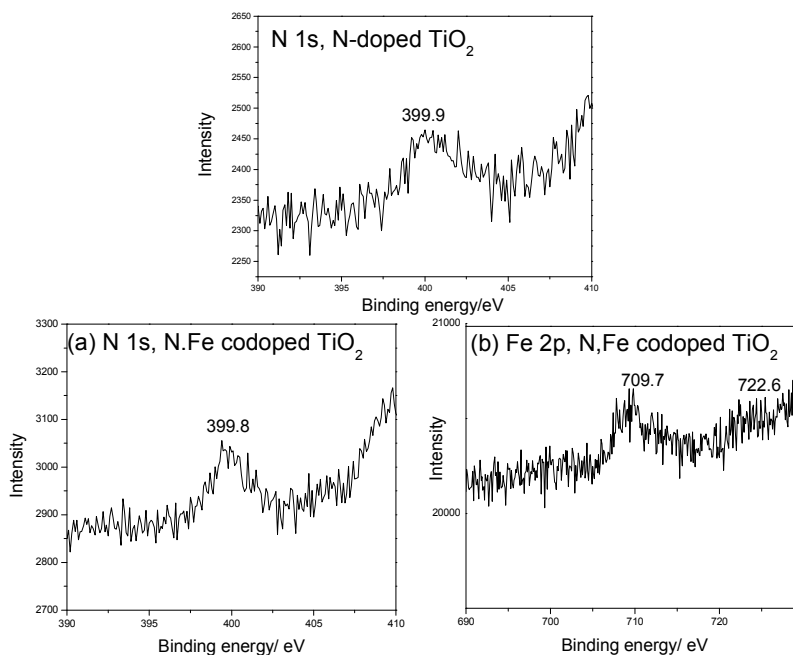


**Fig. 6.** XPS of N-doped TiO<sub>2</sub> and N,Fe codoped TiO<sub>2</sub>

EDS analysis has been used for the elemental analysis of  $\gamma$ -Fe<sub>2</sub>O<sub>3</sub>/N,Fe codoped TiO<sub>2</sub> and the energy peaks corresponding to the elements i.e. N, Fe, O and Ti were observed as shown in

**Fig. 7.**<sup>43</sup>

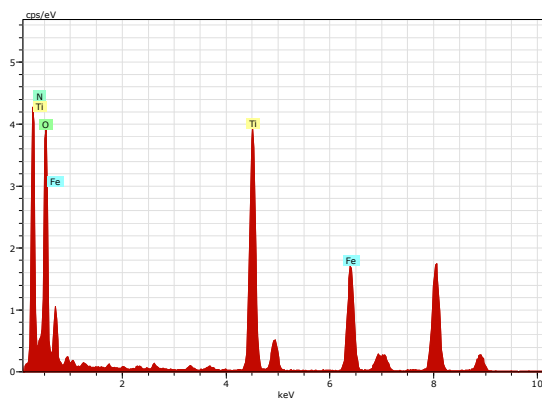


**Fig. 7.** EDS data of (a)  $\gamma$ -Fe<sub>2</sub>O<sub>3</sub>/N,Fe codoped TiO<sub>2</sub>

## 4. Results and discussion

### 4.1. Results of photoactivity test

The RB 4, a textile azo dye, was chosen as a target compound to test the photocatalytic activity of the prepared photocatalysts. The degradation efficiency of the synthesized catalysts was defined as  $C/C_0$ , where  $C$  and  $C_0$  stand for the remnants and initial concentration of the dye respectively. The order of degradation efficiency with respect to the initial rate of reaction for the photocatalytic degradation of the dye under visible light was found to be  $\gamma\text{-Fe}_2\text{O}_3/\text{N,Fe}$  codoped  $\text{TiO}_2 > \text{N,Fe}$  codoped  $\text{TiO}_2 > \text{N-doped TiO}_2 > \text{undoped TiO}_2$  as shown in **Fig. 8**.

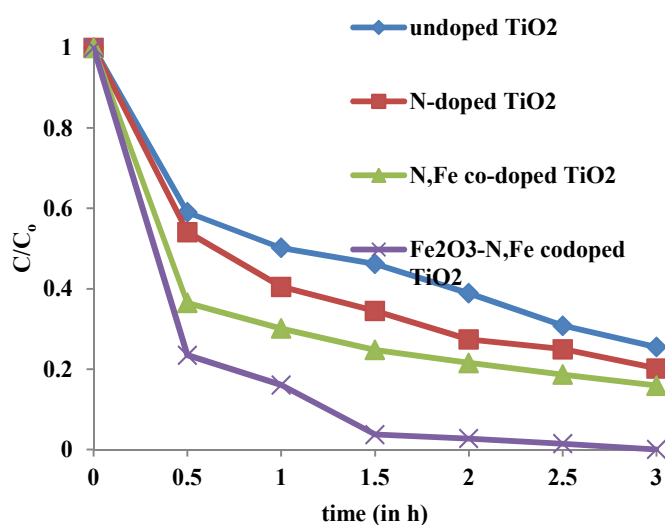


**Fig. 8.** Photocatalytic degradation of RB 4 dye with synthesized catalysts;  $C_0=10$  ppm, catalyst amount= 0.24gm/200ml

#### 4.2. Discussion for mechanism of degradation

In  $\gamma\text{-Fe}_2\text{O}_3/\text{undoped TiO}_2$ , the CB and VB of  $\gamma\text{-Fe}_2\text{O}_3$  is located between CB and VB of  $\text{TiO}_2$  as shown in **Fig. 9**.<sup>44</sup> The electron get excited from VB to CB of  $\gamma\text{-Fe}_2\text{O}_3$  by absorption of visible light, but neither electrons in CB nor holes in VB of the  $\gamma\text{-Fe}_2\text{O}_3$  can be transferred to the CB or VB of  $\text{TiO}_2$  by following pathway **A** and **B**, due to unfavorable energy band matching.

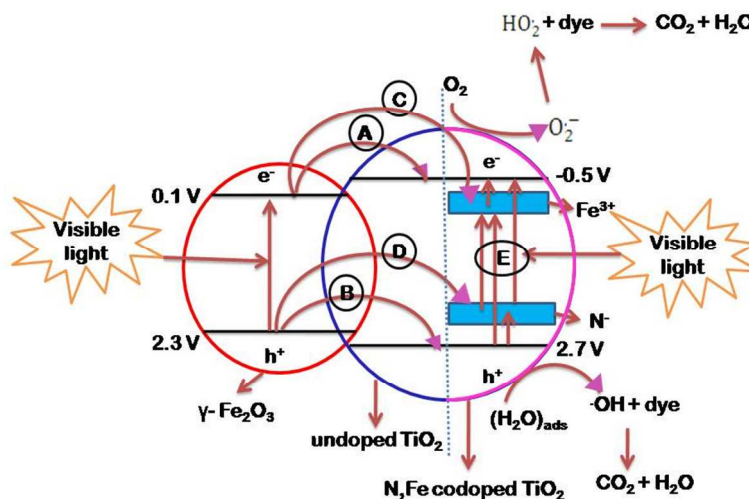
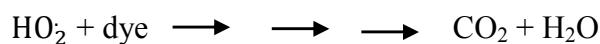
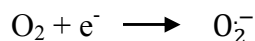


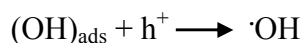
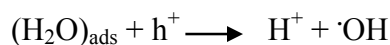
**Fig. 9.** Schematic representation of mechanism involved for degradation of dye in  $\gamma\text{-Fe}_2\text{O}_3/\text{N,Fe}$  codoped  $\text{TiO}_2$  heterojunction

While in  $\gamma\text{-Fe}_2\text{O}_3/\text{N,Fe}$  codoped  $\text{TiO}_2$ , this mismatch of energy bands do not limit the photoactivity of catalyst because codoping with N and Fe induces the formation of new states close to the VB and CB respectively. Due to these newly formed states, the electron and hole mobility from  $\gamma\text{-Fe}_2\text{O}_3$  to impurity band of N,Fe codoped  $\text{TiO}_2$  becomes feasible by pathway C and pathway D respectively as shown in Fig. 9.<sup>45-50</sup> The probable reactions of electrons and holes by pathway C and D are as below, which lead to the degradation of RB 4 dye.

#### Pathway C



#### Pathway D



The narrow band gap of  $\gamma\text{-Fe}_2\text{O}_3/\text{N,Fe}$  codoped  $\text{TiO}_2$  (1.5eV) participates in increasing the quantity of photoinduced electrons and holes by following pathway **E** as shown in **Fig. 7** which leads to enhancement in the utilization of visible light more efficiently for degradation of dye.<sup>51</sup> The high photoactivity of  $\gamma\text{-Fe}_2\text{O}_3/\text{N,Fe}$  codoped  $\text{TiO}_2$  is further facilitated by the large surface area and pure anatase phase because the fast migration of photogenerated electrons and holes from the bulk to surface occurs better in the anatase phase, thus resulting in the low recombination rate of photogenerated charge carriers as reported in literature.<sup>52-54</sup>

### 4.3. Photocatalyst reuse

The magnetic  $\gamma\text{-Fe}_2\text{O}_3$  nanoparticles in  $\text{TiO}_2$  facilitate the separation of photocatalyst that improves the recyclability of the catalyst. The recycling runs were carried out by separating the  $\gamma\text{-Fe}_2\text{O}_3/\text{N,Fe}$  codoped  $\text{TiO}_2$  catalyst under an external magnetic field of intensity 365 Gauss. A mass recovery of  $\sim 98\%$  was achieved with a minor loss. This loss was expected owing to small size. As shown in **Fig. 10**, the photocatalytic activity of catalyst remains almost constant upto 4 runs.

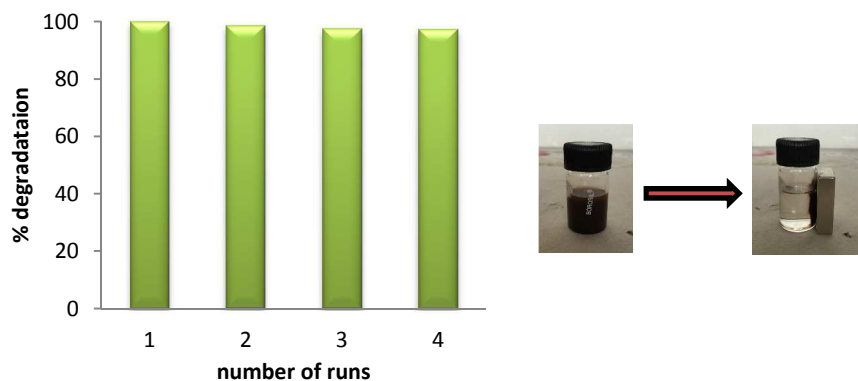


**Fig. 10.** Recycling runs for degradation of RB 4 dye by  $\gamma$ -Fe<sub>2</sub>O<sub>3</sub>/N,Fe codoped TiO<sub>2</sub> ; the inset is a photograph showing separation of catalyst under magnetic field

## 5. Conclusion

In this paper, we have successfully synthesized  $\gamma$ -Fe<sub>2</sub>O<sub>3</sub>/N,Fe codoped TiO<sub>2</sub> which resulted in the formation of a heterojunction and was well characterized. The synthesized  $\gamma$ -Fe<sub>2</sub>O<sub>3</sub>/N,Fe codoped TiO<sub>2</sub> exhibits enhanced photocatalytic activity in comparison to non-magnetic N,Fe codoped TiO<sub>2</sub> and has been well accounted for based on the coupling effect of  $\gamma$ -Fe<sub>2</sub>O<sub>3</sub> and N,Fe codoped TiO<sub>2</sub>, shift in band gap, low electron-hole recombination rate, large surface area and anatase phase. Moreover, the fast magnetic separation and efficient photoactivity of catalyst is advantageous for using the synthesized catalyst in industries for addressing environmental issues.

## Acknowledgements

The generous financial support by PEC University of Technology, Chandigarh and TEQIP (World Bank Project) is gratefully acknowledged. We also thank RSIC, Chandigarh, Dr. Prakash and Dr. R.V. Jasra from Reliance Industries, Gujarat for analysis.

## References

1. Y. Zhang, J. C. Crittenden, D. W. Hand and D. L. Perram, *Environ. Sci. Technol.*, 1991, **28**, 435-442.
2. M. R. Hoffmann, S. T. Martin, W. Choi and D. W. Bahnemann, *Chem. Rev.*, 1995, **95**, 69-96.
3. J. Zhao, T. Wu, K. Wu, K. Oikawa, H. Hidaka and N. Serpone, *Environ. Sci. Technol.*, 1998, **32**, 2394-2400.
4. H. Li, X. He, Z. Kang, H. Huang, Y. Liu, J. Liu, S. Lian, C. H. A. Tsang, X. Yang and S. T. Lee, *Angew. Chem. Int. Ed.*, 2010, **49**, 4430-4434.
5. X. Chen and S. S. Mao, *Chem. Rev.*, 2007, **107**, 2891-2959.
6. W. Q. Fang, Z. Huo, P. Liu, X. L. Wang, M. Zhang, Y. Jia, H. Zhang, H. Zhao, H. G. Yang and X. Yao, *Chem. Eur. J.*, 2014, **20**, 11439-11444.
7. D. Qi, M. Xing and J. Zhang, *J. Phys. Chem. C.*, 2014, **118**, 7329-7336.
8. S. Sridhar, A. Viswanathan, K. Venkateswarlu, N. Rameshbabu and N. L. Parthasarathi, *J. Porous Mater.*, 2015, **22**, 545-557.
9. Y. Wang, R. Zhang, J. Li, L. Li and S. Lin, *Nanoscale Res. Lett.*, 2014, **9**, 46-54.
10. J. M. Valero, S. Obregon and G. Colon, *ACS Catal.*, 2014, **4**, 3320-3329.
11. N. Khakpash, A. Simchi and T. Jafari, *J. Mater. Sci-Mater. Electron.*, 2012, **23**, 659-667.
12. L. C. Jia, C. C. Wu, S. Han, N. Yao, Y. Y. Li, Z. B. Li, B. Chi, J. Pu and L. Jian, *J. Alloys Compd.*, 2011, **509**, 6067-6071.
13. A. T. Kuvarega, R. W. M. Krause and B. B. Mamba, *J. Phys. Chem. C.*, 2011, **115**, 22110-22120.
14. X. Li, Z. M. Chen, Y. C. Shi and Y. Y. Liu, *Powder Technol.*, 2011, **207**, 165-169.
15. K. S. Rane, R. Mhalsiker, S. Yin, T. Sato, K. Cho, E. Dunbar and P. Biswas, *J. Solid State Chem.*, 2006, **179**, 3033-3044.
16. H. M. Chen, C. H. Deng and X. M. Zhang, *Angew. Chem. Int. Ed.*, 2010, **49**, 607-611.
17. P. M. Rao and X. L. Zheng, *Nano Lett.*, 2011, **11**, 2390-2395.
18. V. Tyrpeki, J. P. Vejpravova and A. G. Roca, *Appl. Surf. Sci.*, 2011, **257**, 4844-4848.
19. M. S. Lucas, P. B. Tavares, J. A. Peres, J. L. Faria, M. Rocha, C. Pereira and C. Freire, *Catal Today.*, 2013, **209**, 116-121.
20. R. Chalasani and S. Vasudevan, *ACS Nano*, 2013, **7**, 4093-4104.

21. B. Cui, H. Peng, H. Xia, X. Guo and H. Guo, *Sep. Purif. Technol.*, 2013, **103**, 251-257.
22. M. He, D. Li, D. Jiang and M. Chen, *J. Solid State Chem.*, 2012, **192**, 139-143.
23. M. Pelaez, B. Baruwati, R. S. Varma, R. Luque and D. D. Dionysiou, *Chem. Comm.*, 2013, **49**, 10118-10120.
24. L. Yu, X. Yang, J. He, Y. He and D. Wang, *Sep. Purif. Technol.*, 2015, **144**, 107-113.
25. J. R. Jeong, S. J. Lee, J. D. Kim and S. C. Shin, *Phys. Status Solidi B*, 2004, **241**, 1593-1596.
26. S. H. Xuan, Y. J. Wang, J. C. Yu and K. C. Leung, *Chem. Mater.*, 2009, **21**, 5079-5087.
27. E. M. Patterson, C. E. Shelden and B. H. Stockton, *Appl. Optics*, 1977, **13**, 729-732.
28. Y. Su, Y. Xiao, Y. Li, Y. Du and Y. Zhang, *Mater. Chem. Phys.*, 2011, **126**, 761-768.
29. M. Niyafar, A. Hasanpour, H. Mohammadpour and J. Anighian, *Phys. Status Solidi A*, 2013, **210**, 1190-1194.
30. K. M. Parida and B. Naik, *J. Colloid Interface Sci.*, 2009, **333**, 269-276.
31. X. X. Yu, S. W. Liu and J. G. Yu, *Appl. Catal. B: Environ.*, 2011, **104**, 12-20.
32. A. Zielinska, E. Kowalska and J. W. Sobczak, *Sep. Purif. Technol.*, 2010, **45**, 155-162.
33. A. Ibrahim, S. K. J. A. Ani, *Czech. J. Phys.*, 1994, **44**, 785-797.
34. Y. Cong, J. Zhang, F. Chen, M. Anpo and D. He, *J. Phys. Chem. C.*, 2007, **111**, 10618-10623.
35. R. Asahi, T. Morikawa, T. Ohwaki, K. Aoki and Y. Taga, *Sci.*, 2001, **293**, 269-271.
36. H. Liu, H. K. Shon, X. Sun, S. Vigneswaran and H. Nan, *Appl. Surf. Sci.*, 2011, **257**, 5813-5819.
37. R. Khan and T. J. Kim, *J. Hazard. Mater.*, 2009, **163**, 1179-1184.
38. J. Yang, X. Wang, J. Dai and J. Li, *Ind. Eng. Chem. Res.*, 2014, **53**, 12575-12586.
39. A. Banisharif, A. A. Khodadadi, Y. Mortazavi, A. A. Firooz, J. Beheshtian, S. Agah and S. Menbari, *Appl. Catal. B: Environ.*, 2015, **165**, 209-221.
40. S. Livraghi, M. R. Chierotti, E. Giamello, G. Magnacca, M. C. Paganini, G. Cappelletti and C. L. Bianchi, *J. Phys. Chem. C*, 2008, **112**, 17244-17252.
41. F. Napoli, M. Chiesa, S. Livraghi, E. Giamello, S. Agnoli, G. Granozzi, G. Pacchioni and C. Di Valentin, *Chem. Phys. Lett.*, 2009, **477**, 135-138.
42. S. Sato, R. Nakamura and S. Abe, *Appl. Catal. A*, 2005, **284**, 131-137.
43. M. Montazer, A. Behzadnia and E. Pakdel, *J. Photochem. Photobiol B*, 2011, **103**, 637-640.

44. S. B. Rawal, S. Bera, D. Lee, D. J. Jang and W. I. Lee, *Catal. Sci. Technol.*, 2013, **3**, 1822-1830.
45. Y. Bessekhoad, N. Chaoui, M. Trzpit, N. Ghazzal, D. Robert and J. V. Weber JV, *J. Photochem. Photobiol. A*, 2006, **183**, 218-224.
46. U. I. Gaya and A. H. Abdullah, *J. Photochem. Photobiol. C.*, 2008, **9**, 1-12.
47. S. B. Rawal, A. K. Chakraborty, Y. J. Kim, H. J. Kim and W. I. Lee, *RSC Adv.*, 2012, **2**, 622-630.
48. Y. J. Kim, B. Gao, S. Y. Han, M. H. Jung, A. K. Chakraborty, T. Ko, C. Lee and W. I. Lee, *J. Phys. Chem. C.*, 2009, **113**, 19179-19184.
49. S. Shamaila, A. K. L. Sajjad, F. Chen and J. Zhang, *J. Colloid Interface Sci.*, 2011, **356**, 465-472.
50. H. Gnaser, M. R. Savina, W. F. Chalaway, C. E. Tripa, I. V. Veryovkin and M. J. Pellin, *Int. J. Mass Spectrom.*, 2005, **245**, 61-67.
51. Y. Cong, J. Zhang, F. Chen, M. Anpo and D. He, *J. Phys. Chem. C.*, 2007, **111**, 10618-10623.
52. J. Joo, J. Shim, H. Seo, N. Jung, U. Weisner, J. Lee and S. Jeon, *Anal. Chem.*, 2010, **82**, 3032-3037.
53. J. Joo, Y. Ye, D. Kim, J. Lee and S. Jeon, *Mat. Lett.*, 2013, **93**, 141-144.
54. J. Zhang, P. Zhou, J. Liu and J. Yu, *Phys. Chem. Chem. Phys.*, 2014, **16**, 20382-20386.